Time-delayed single quantum repeater node for global quantum communications with a single satellite

Mustafa Gündoğan,[1,*] Jasminder S. Sidhu,[2] Daniel K. L. Oi,[2] and Markus Krutzik[1,3]

[1] *IRIS and Institut für Physik, Humboldt-Universität zu Berlin, Newtonstr. 15, Berlin 12489, Germany*
[2] *SUPA Department of Physics, University of Strathclyde, John Anderson Building, 107 Rottenrow East, Glasgow, G4 0NG, UK*
[3] *Ferdinand-Braun-Institut (FBH), Gustav-Kirchoff-Str.4, 12489 Berlin*

Quantum networking on a global scale is an immensely challenging endeavor that is fraught with significant technical and scientific obstacles. While various types of quantum repeaters have been proposed they are typically limited to distances of a few thousand kilometers or require extensive hardware overhead. Recent proposals suggest that space-borne quantum repeaters composed of a small number of satellites carrying on-board quantum memories would be able to cover truly global distances. In this paper, we propose an alternative to such repeater constellations using an ultra-long lived quantum memory in combination with a second memory with a shorter storage time. This combination effectively acts as a time-delayed version of a single quantum repeater node. We investigate the attainable finite key rates and demonstrate an improvement of at least three orders of magnitude over prior single-satellite methods that rely on a single memory, while simultaneously reducing the necessary memory capacity by the same amount. We conclude by suggesting an experimental platform to realize this scheme.

I. INTRODUCTION

Long-distance ($> 10^3$ km) quantum networking is a challenging but yet a very important task that has garnered an intense attention from the community. Unlike in classical communications, deterministic amplifiers are not allowed in quantum mechanics [1, 2] which makes the task a unique scientific and technological problem. Currently, fibre-based long-distance quantum communication experiments are limited to around few hundred kilometers [3] which was made possible due to new techniques such as the twin-field quantum key distribution (QKD) [4] and developments in low-loss fibre and low-noise single photon detector technologies. However, pushing this limit beyond $\sim 10^3$ km requires more radical approaches, such as quantum repeaters (QRs) or entanglement distribution from space via free-space channels.

QRs based on active error correction have been shown to be capable of reaching global distances albeit with enormous technical overhead: repeater nodes, each of which contains a small-scale quantum processor, must be separated by very short distances, i.e 1-2 km [5]. On the other hand, QRs based on heralded generation of entanglement [6, 7] can have their nodes placed every several tens of kms but their total range is limited to around a few thousand km [7–10].

The other approach towards pushing the direct communication limit is to use free-space channels instead of fibre links. In this way, the exponential scaling of the loss in fibres are replaced with the (mainly) polynomial scaling of the free-space channel loss. Recent years saw the first milestone experiments: MICIUS satellite [11] has demonstrated ground-space teleportation [12], quantum key distribution (QKD) with entangled photons across 1120 km [13], intercontinental QKD operated in trusted node [14] and the integration of satellite links into long-distance, trusted node ground networks [15]. Impressive as they are, the range of these experiments are limited to the line-of-sight distance of the satellite which depends on the orbital height (~ 2000 km for $h = 500$ km) unless the satellite operates as a trusted node [14, 16].

There are recent proposals towards creating satellite networks for fully global ($d > 10^4$ km) coverage. The first efforts were concentrated on hybrid, space-ground QRs [17] where the quantum memories (QM) are located in ground stations, and this scheme was recently extended towards a fully satellite-based QRs [18, 19] where the QMs are located on board orbiting satellites [20]. These work demonstrate that entanglement distribution across the whole globe would be possible with a network of satellites equipped with QMs and entangled photon pair sources. It was shown that a storage time of around <1 s could be sufficient to reach global distances [19] whereas intercontinental distances of > 8000 km would be possible with memory times of around 100 ms [19, 21].

An alternative to networked entanglement distribution is physically transporting [22] the qubits given that qubit lifetime is longer than the transport time. This can either be done via active quantum error correction [23] or by utilizing ultra-long lifetime (ULL) QMs [24, 25]. In this work we propose a time-delayed version of a single-node quantum repeater [26–28] architecture that can be implemented with a single orbiting satellite that carries an ULL QM in combination with a shorter lived (∼ms) one. Our scheme extends the performance and reduces the hardware requirements of a related proposal [24] by several orders of magnitude.

This manuscript is organized in the following way: we first outline the protocol with two quantum memories and highlight the differences between the earlier, single-

* mustafa.guendogan@physik.hu-berlin.de

memory scheme. We then present finite key analysis of this scheme and from there deduce the required memory performances. Finally, we discuss possible implementations of this scheme and provide an experimental guideline.

II. PROTOCOL WITH TWO QUANTUM MEMORIES

An earlier work proposed using ULL QMs for global quantum communications [24]. In that scheme, a satellite is equipped with an ULL QM together with an entangled photon pair source. The source sends one of the photons to a ground station and its pair is stored in the on-board QM. The QM is read out when the satellite is flying over the second ground station at a later time and the photon is transmitted to this ground station. On the other hand, our scheme requires two QMs on-board the satellite with differing storage time requirements. The first one needs to have $\tau_{QM1} > 1$ h with a high multimode capacity whereas the second memory only needs $\tau_{QM2} \sim 2L/c$, where L is the distance between the satellite and the ground station. Having a single QM on board would limit the keyrate to η_{ch}^2 whereas the addition of the second QM would enhance the scaling to $\sim \eta_{ch}$, where η_{ch} is average single channel loss in the absence of detector dark counts and stray light from the atmosphere. In this respect our scheme can be regarded as the time delayed version of a single quantum repeater node [26–28] that enhances the achievable key rate and distance, i.e. the maximum tolerable loss.

A simple schematic of our scheme is presented in Figure 1. The protocol starts with the source emitting entangled photon pairs at a rate s when the satellite starts its pass over the ground station A. One of these photons is resonant with the QM1 and is immediately stored. The other pair is sent to the ground station A through the atmospheric channel. If this photon is lost along the path then the stored photon in the QM1 is erased and it is only kept in the memory when A successfully detects the photon in a BB84 (BBM92) setting. After the flyover is completed the satellite continues to travel in its orbit. The source again starts emitting photon pairs at rate s when it is flying over ground station B. One of the pairs is sent to ground station B whereas the other photon is stored in QM2. If a successful BB84 measurement is done in ground station B then the corresponding photon from QM2 is immediately retrieved together with a photon stored in QM1 which is then followed by a Bell state measurement (BSM) on these photons. Here, similar to [26, 27], the result of the BSM is then transmitted to station B. If B performed the BB84 measurement in Z (X) basis then a bit flip is applied to the measurement if the BSM resulted in $|\Psi^+\rangle$ or $|\Psi^-\rangle$ ($|\Phi^+\rangle$ or $|\Phi^-\rangle$). Although we consider a QM paired with an entangled photon pair source [9, 29], the same protocol can be realized with a DLCZ-type memory, where the QM can emit a single photon entangled with its internal atomic states [8].

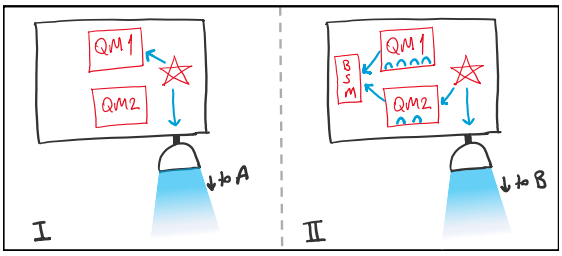

FIG. 1. The protocol with two QMs. (I) One photon of the pair is stored in the long-lived QM1 whereas its pair is sent to the ground station A. (II) When the satellite is over the ground station B the source now sends a photon to the corresponding ground station and the other photon is stored in QM2. At the same time BSM is performed on the photons stored earlier.

III. KEY RATE ANALYSIS

Key rates are usually calculated in the asymptotic limit [30], i.e. when the raw key has an infinite length. However, for the case of low Earth orbits (LEO) the limited contact time between the satellite and the ground stations would make this approximation invalid. In this case the finite block size effects should be taken into account. Although it was refined later in Ref [31] by appropriately accounting for the cost of parameter estimation, we follow the approach used in Ref. [13] for its simplicity for this purpose, but assign a tighter security parameter to maintain the security of finite keys to calculate the key length as a function of overall channel loss. Key length in Z basis is then given by

$$\begin{aligned} L_Z =& n_Z - n_Z h\left[\frac{e_X + \sqrt{\frac{(n_Z+1)\log\left(\frac{1}{\epsilon_{\text{sec}}}\right)}{2n_X(n_X+n_Z)}}}{1-\Delta}\right] \\ &- f_e n_Z h\left(e_Z\right) - n_Z\Delta - \log\frac{2}{\epsilon_{\text{cor}}\epsilon_{\text{sec}}^2}. \end{aligned} \tag{1}$$

The key length calculation for X basis is similar to Eq. 1 thus the total key length becomes $L = L_X + L_Z$. Here ϵ_{sec} and ϵ_{sec} are levels of secrecy and correctness so that the protocol is ϵ-secure with $\epsilon \geq \epsilon_{\text{sec}} + \epsilon_{\text{sec}}$ [13]. Here Δ is a factor to account for the mismatch of different detector efficiencies and n_Z and n_X are coincidences in Z and X bases.

The QBERs in X and Z bases are given by [26]

$$\begin{aligned} e_X =& \lambda_{\text{BSM}}\alpha_A\alpha_B\left[\epsilon_m\left(1-\epsilon_{\text{dp}}\right) + \left(1-\epsilon_m\right)\epsilon_{\text{dp}}\right] \\ &+ \frac{1}{2}\left[1 - \lambda_{\text{BSM}}\alpha_A\alpha_B\right] \end{aligned} \tag{2}$$

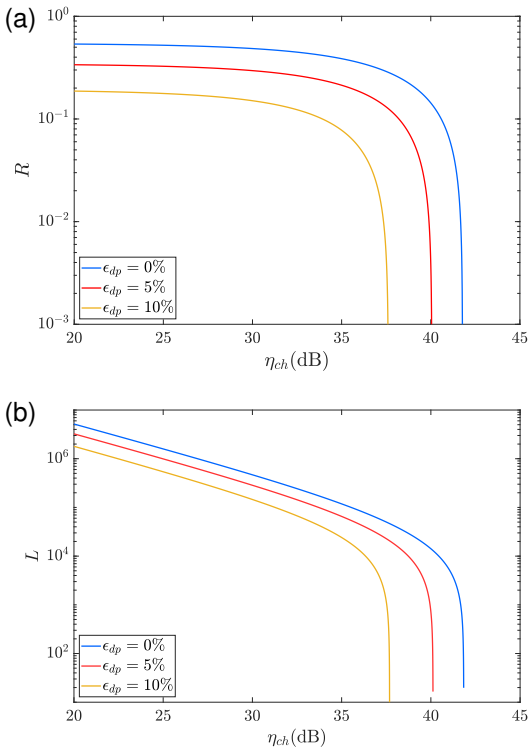

FIG. 2. Achievable secret key rate per distributed pair, R, (a) and secret key length, L, (b) as a function of average channel loss with different memory dephasing values. Other parameters are given in the text.

and

$$e_Z = \lambda_{\mathrm{BSM}}\alpha_A\alpha_B\epsilon_m + \frac{1}{2}\left[1 - \lambda_{\mathrm{BSM}}\alpha_A\alpha_B\right]. \qquad (3)$$

Here λ_{BSM} is the success probability of the BSM, α_k is the probability of a real detection event in ground station k (Appendix A), ϵ_m is the misalignment error and ϵ_{dp} is the dephasing during the storage in memories. Ensemble based memories that we consider in this work have been shown to preserve the phase independent of the storage time [32–34]. This is due to the fact that reemission of the stored information relies on the rephasing of these excitations [35] which means that any dephasing will result in lower efficiency operation all the while maintaining a high fidelity. We assume a memory efficiency of around 60 % at 90 minutes following the observed $T_2 = 6$ h in a Europium doped crystal [25, 36] (details are in Sec. IV). We further assume $\lambda_{\mathrm{BSM}} = 0.98$ [26, 27].

Figure 2a shows the achievable key rate per distributed pair, R, as a function of average channel loss, η_{ch}, calculated for a 200 s flyover time for different memory dephasing values, ϵ_{dp}. Since the key rate formula only depends on the overall loss, this figure can serve a guide for any scenario with a given, total channel loss. For these simulations we assume $s = 5$ MHz which is mainly limited by the narrow memory bandwidth, $\epsilon_m = 2\%$ and quite a tight $\epsilon_{corr} = \epsilon_{sec} = 5 \times 10^{-12}$ [37]. The other details are given in Appendices. We see that up to 42 dB of average loss can be tolerated with ideal QMs that do not introduce any dephasing, ϵ_{dp}. For $\epsilon_{dp} = 5\%$ one can achieve finite key rates up to 40 dB loss. In order to put this value in perspective Ref. [34] reported $\epsilon_{dp} \sim 8\%$ for 1 h storage time with classical pulses. Fig. 2b shows that finite key lengths ($L = L_X + L_Z$) of around $\sim 10^5$ can be obtained with an average single channel loss of 30 dB which is similar to that reported in Ref. [13].

Having two QMs on board has a significant advantage over schemes that rely on a single QM [24]. Figure 3 shows this difference between single- and two-memory schemes for $\epsilon_{dp} = 5\%$. For a single-memory scheme 31 dB average loss seems to be the maximum tolerable loss beyond which meaning full generation becomes impossible. The finite block size effect becomes important especially after ~ 27 dB loss. Figure 3b explicitly demonstrates the advantage of two-memory scheme over its single memory counterpart. It not only supports much higher losses, but also provides orders of magnitude higher secret key lengths. The other important aspect is the smaller slope of the curve for the two-memory case which clearly shows the repeater-like enhancement. Figure 3c shows the effect of incoherent clicks, p_d, on the detector (see Appendix B for details). It is striking that the two-memory scheme is much more resilient to noise, almost a factor of three over the single memory case.

IV. MEMORY ARCHITECTURE

The scheme requires the memories to have i) large storage, i.e. multimode capacity, N and ii) long storage times. The required N is given by the $n = n_Z + n_X$ for the two-memory protocol whereas the storage time has to be larger than the orbital period (~ 90 min for LEO). $N \sim 200$ has recently been demonstrated in several experiments: laser cooled gases [38] with spatial multiplexing and rare-earth ion doped crystal (REID) memories with a combination of temporal and spectral multiplexing [39]. Among these, REIDs have the long memory lifetime capacity required by the protocol we propose. REIDs have an optical transition between $4f$ electronic orbitals which are located within totally filled $5s$ or $5d$ shells [40]. This effectively shields the optically active $4f$ orbitals from external disturbances and thus results in very sharp optical lines connected to long-lived ground states. Furthermore their large inhomogenous broadening (γ_{inh}) can be used as a resource to realize memory protocols based on rephasing of the stored excitations. Among different REIDs Europium has an hyperfine lifetime of around three weeks [41, 42] and coherence time of 6 h was demonstrated [36]. Recently, this system was used for coherent storage of bright pulses with a storage time > 1 h [34] with the atomic frequency comb (AFC) protocol [35]. Furthermore, recent advances towards developing such QMs with built-in fibre couplers [43, 44]

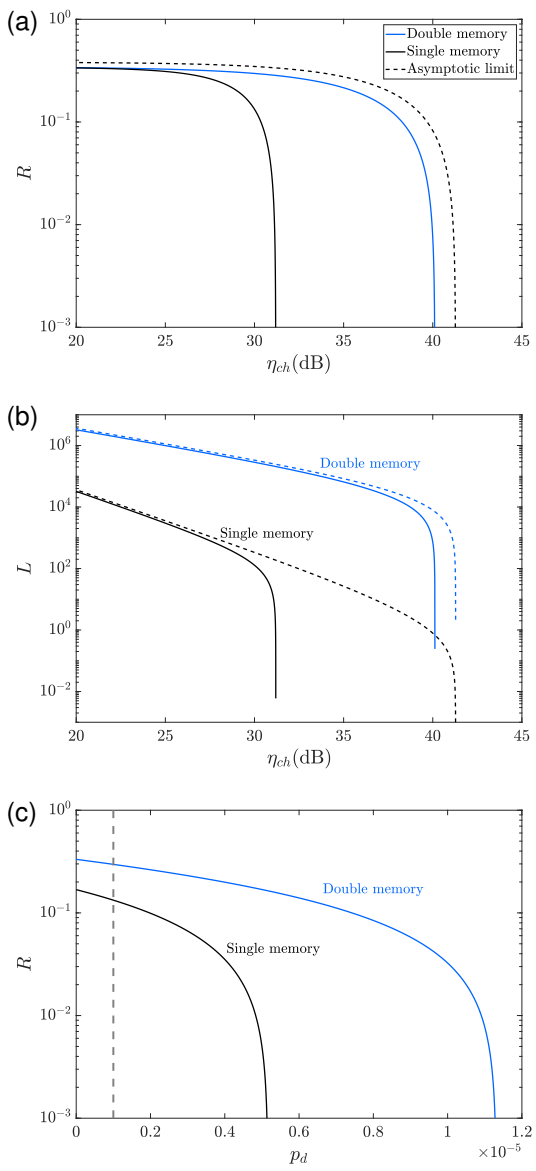

FIG. 3. Comparison between double- and single-memory schemes. (a) Finite key rate per distributed pair and (b) total finite key length as a function of average single channel loss. Dashed lines indicate the asymptotic limits. (c) Finite key rate per distributed pair with changing total incoherent noise for $\eta_{ch} = 30$ dB. Vertical dashed line indicates $p_d = 10^{-6}$, the value we assumed in the rest of the calculations.

would enable enhanced coupling between the optical free space and memory modes.

We identify that AFC protocol could satisfy the strict multimode requirements imposed by our scheme. AFC relies on creating a comb shaped absorption profile by optical pumping within the inhomogenous profile of the ensemble. It was shown that the number of temporal modes that can be stored with this protocol is $\sim N_{AFC}/6$, where N_{AFC} is the number absorption peaks within the comb [35]. With a bandwidth of a few MHz, we can expect to create an AFC that could store $N_t \sim 10^2$ temporal modes with $N_{AFC} \sim 600$ [45]. REIDs are also suitable for large spectral multiplexing [39, 46] capability due to the inhomogenous broadening they posses: up to $N_f \sim 10^3$ spectral modes can be stored within an optical transition with $\gamma_{\text{inh}} \sim 10$ GHz. Finally, laser waveguide writing techniques [45, 47] may allow creating $N_s \sim 100 \times 100$ arrays of spatial modes within a single crystal, thus putting the total number of available modes to $N_{\text{Mem}} = N_t \times N_f \times N_s \sim 10^9$. This hypothetical value is well beyond the required capacity of $N \sim 5{\times}10^5$ for 30 dB average channel loss in combination with $\eta_{mem} = 0.6$ and $\eta_{det} = 0.8$. These quantum memories require cryogenic operation at temperatures < 4 K. Although this is one of the technical challenges for deploying such devices in space, recent efforts to develop satellite-borne cryostats for quantum optical applications are promising. [48–50]. Highly efficient, low-noise single photon counters are also available. We should note that timing jitter of the detectors (< 1 ns) would not affect the measurement as the signal photons would need to be around 200 ns long. We should note that QM2 can be implemented with the same protocol which would also make sure the indistinguishability of photons for the BSM. In Appendix C we demonstrate that this protocol, with $s = 5$ MHz, is superior to QKD from the geostationary orbit with photon pair rates of 1 GHz.

V. CONCLUSIONS

In this study, we introduce a quantum communication protocol that utilizes the physical transportation of stored qubits in ULL QM on board an orbiting satellite. This protocol aims to reduce the technical requirements for operating global quantum networks. Our results demonstrate that using two QMs instead of one significantly increases the maximum channel loss that can be tolerated while reducing the required multimode capacity from around $\sim 10^8$ [24] to $\sim 10^5$. We anticipate that the necessary storage time and multimode capacity can be achieved in the near future. Additionally, utilizing more recent finite key calculations that specifically address space-based QKD scenarios can potentially increase calculated secret key lengths by approximately ∼10%. Finally, ULL QMs in orbit may also serve as useful probes to investigate the intersection of quantum physics and general relativity [51] and enable human-assisted Bell tests across Earth-Moon distances [11, 52, 53].

VI. ACKNOWLEDGEMENTS

We thank S. Wittig for bringing the earlier work [24] to our attention during discussion at an early stage of this work and E. İmre for useful discussions on satellite communication techniques. MG and MK acknowledge the support from DLR through funds provided

by BMWi (OPTIMO, No. 50WM1958 and OPTIMO-II, No. 50WM2055), MG is further supported by funding from the European Union's Horizon 2020 research and innovation programme under the Marie Skłodowska-Curie grant agreement No. 894590 (QSPACE). DKLO is supported by the EPSRC Researcher in Residence programme (EP/T517288/1). JSS, and DKLO acknowledge the travel support by the EU COST action QTSpace (CA15220). Funding was provided by the UK Space Agency through the National Space Technology Programme (NSTP3-FT-063 "Quantum Research CubeSat", NSTP Fast Track "System Integration & Testing of a CubeSat WCP QKD Payload to TRL5"), EPSRC Quantum Technology Hub in Quantum Communication Partnership Resource (EP/M013472/1) and Phase 2 (EP/T001011/1), and Innovate UK (EP/S000364/1). This work was supported by the EPSRC International Network in Space Quantum Technologies INSQT (grant ref: EP/W027011/1).

Appendix A: Key rate calculation details

Satellite based quantum communications present several challenges with respect to its fibre-based counterpart. These are mainly: high, dynamic channel loss and the relatively short contact time (∼min for LEO) between the sender and receiver stations. With these constraints in mind, we also take into account the finite key effects on the final, generated secret lengths.

Final secret key length, $L_{X,Z}$, is given in Eq. 1. We see from Equations 2 and 3 that the physical factors that contribute to the QBERs, e_X and e_Z are λ_{BSM}, α_k, ϵ_{dp} and ϵ_m. Among these only the memory dephasing, ϵ_{dp} contributes to error in the X basis.

Here, α_k is the probability of registering a real click in ground station k [26]. This probability then decreases with any incoherent, noise click at the detector and depends on total detection probability η:

$$\alpha(\eta) = \frac{\eta(1-p_d)}{1-(1-\eta)(1-p_d)^2}. \tag{A1}$$

Here, $\eta = \eta_{ch}\eta_{det}\eta_{mem}$ where η_{ch} is average channel transmission; η_{det} is detection efficiency and η_{mem} is the combined memory write-in and read-out efficiency. p_d is the probability of any incoherent click on the detector during the detection time window. Here $p_d = \eta_{ch}p_n + p_{bg} + p_{dc}$. p_n is the noise added by memory when there is no input pulse; p_{bg} is the background noise probability and p_{dc} is detector dark count probability. These contributions are further detailed in the next section.

Δ in Eq. 1 accounts for the efficiency mismatch between different detectors. Adding a filter with small attenuation, δ_i, to the ith detector would result in $\Delta = 1 - 1/(1+\delta)$ [13]. In this work we assume $\Delta \sim 2\%$.

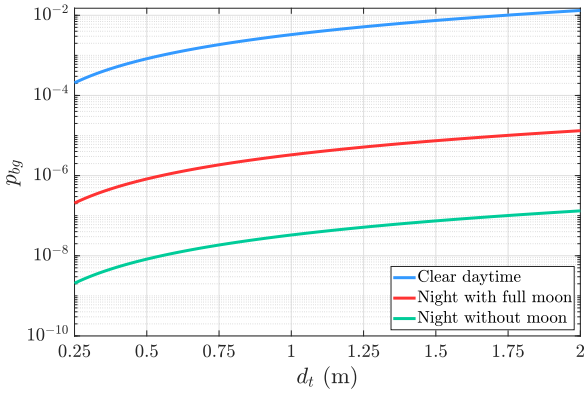

FIG. 4. Background click probability, p_{bg}, as a function of receiver telescope diameter. Details and parameters are given in Appendix B.

Appendix B: Incoherent clicks

Any incoherent click will have a detrimental effect of the maximum tolerable loss. These can be grouped into three:

- Detector dark counts: dark count rate of around 10 Hz is readily achievable with detectors at room temperature whereas < 1 Hz is possible with cryogenically cooled superconducting single photon detectors.

- Noise coming from memory operation: long-lived QMs usually add noise to the output signal. This is due to a combination of several factors such as imperfect preparation of the memory, leakage from the strong control pulses and resonant four wave mixing noise. The probability of emitting a noise photon per storage trial, p_n, is around 10^{-3} for REID QMs [54, 55] whereas $\sim 10^{-4}$ has been achieved with laser cooled gases [56].

- Background light. Detailed treatment of background light under different conditions (total dark skies, full moon, daylight etc.) is given elsewhere [21, 57]. Fig. 4 shows the expected background noise photon with different scenarios. Relevant parameters are as follows: spectral filter bandwidth: 20 GHz; central wavelength: 580 nm; detection window: 500 ns; field of view: 6.14×10^{-5} Sr which is similar to observed area of the Moon in the sky and brightness of the sky: 150 W m^{-2}Srμm. Background noise photons can be reduced further by employing an even narrower spectral filter (down to $\sim$ 10 MHz should be possible), however in that case the filter has to be actively tuned to compensate for the Doppler shift due to satellite's orbital movement. Furthermore, one can design the photon pair source such that photons sent to the ground stations would lie within a Fraunhofer line

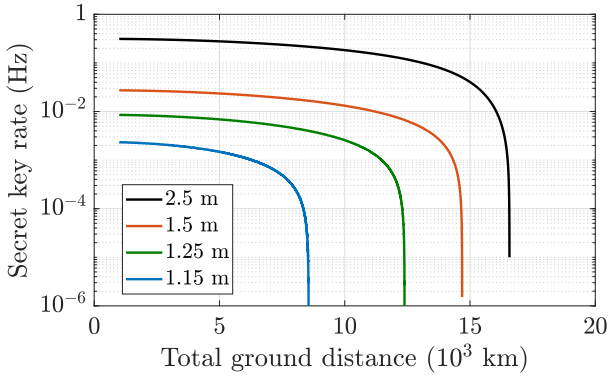

FIG. 5. Achievable key rates from a GEO with an ent-QKD protocol without any QM with different receiver telescope radii. Other parameters are given in Sec. C.

to enable daylight operation [58]. This option would not be possible in a single memory scheme as the photons stored in the memory would have to be transmitted to a ground station later on.

Appendix C: Comparison with a QKD from geostationary orbit (GEO)

Following Refs. [19, 59], in this section we present calculations of entanglement-based QKD without any QMs from a satellite in GEO. We assume a source rate of 1 GHz, sender telescope radii of 0.15 m, dark count probability of 10^{-6}, wavelength of 852 nm (atmospheric transmissivity at 852 nm is around 25% higher than it is for 580 nm [19]) and beam divergence of 5 μrad with varying receiver telescope radii from 1.15 m to 2.5 m (Fig. 5). We follow our earlier work [19, 21] for the channel modelling. This calculation does not include tracking errors and turbulence effects thus represent a best case scenario. With this, we see that losses prevent achieving fully global distances, even with 2.5 m diameter receiver telescopes. In order to compare this GEO scenario with the presented protocol in this manuscript one needs to calculate the number of flyovers over a given pair of ground stations. Along these lines, in Ref. [24] a hypothetical link between Adelaide and Brussels (total distance 15.9×10^3 km) is considered for which the authors find 1257 flyover pairs within a year. Based on an average channel loss of 35 dB, our analysis shows that deploying a single satellite equipped with a ULL QM using the protocol in this manuscript would result in a performance gain of $\sim 2.5 \times 10^2$ over the GEO scenario.

[1] D. Dieks, Physics Letters A **92**, 271 (1982).
[2] W. K. Wootters and W. H. Zurek, Nature **299**, 802 (1982).
[3] J.-P. Chen, C. Zhang, Y. Liu, C. Jiang, W. Zhang, X.-L. Hu, J.-Y. Guan, Z.-W. Yu, H. Xu, J. Lin, M.-J. Li, H. Chen, H. Li, L. You, Z. Wang, X.-B. Wang, Q. Zhang, and J.-W. Pan, Phys. Rev. Lett. **124**, 070501 (2020).
[4] M. Lucamarini, Z. L. Yuan, J. F. Dynes, and A. J. Shields, Nature **557**, 400 (2018).
[5] S. Muralidharan, J. Kim, N. Lütkenhaus, M. D. Lukin, and L. Jiang, Phys. Rev. Lett. **112**, 250501 (2014).
[6] L. Childress, J. M. Taylor, A. S. Sørensen, and M. D. Lukin, Phys. Rev. Lett. **96**, 070504 (2006).
[7] N. Sangouard, C. Simon, H. de Riedmatten, and N. Gisin, Rev. Mod. Phys. **83**, 33 (2011).
[8] L.-M. Duan, M. D. Lukin, J. I. Cirac, and P. Zoller, Nature **414**, 413 (2001).
[9] C. Simon, H. de Riedmatten, M. Afzelius, N. Sangouard, H. Zbinden, and N. Gisin, Phys. Rev. Lett. **98**, 190503 (2007).
[10] S. E. Vinay and P. Kok, Phys. Rev. A **95**, 052336 (2017).
[11] C.-Y. Lu, Y. Cao, C.-Z. Peng, and J.-W. Pan, Rev. Mod. Phys. **94**, 035001 (2022).
[12] J.-G. Ren, P. Xu, H.-L. Yong, L. Zhang, S.-K. Liao, J. Yin, W.-Y. Liu, W.-Q. Cai, M. Yang, L. Li, K.-X. Yang, X. Han, Y.-Q. Yao, J. Li, H.-Y. Wu, S. Wan, L. Liu, D.-Q. Liu, Y.-W. Kuang, Z.-P. He, P. Shang, C. Guo, R.-H. Zheng, K. Tian, Z.-C. Zhu, N.-L. Liu, C.-Y. Lu, R. Shu, Y.-A. Chen, C.-Z. Peng, J.-Y. Wang, and J.-W. Pan, Nature **549**, 70 (2017).
[13] J. Yin, Y.-H. Li, S.-K. Liao, M. Yang, Y. Cao, L. Zhang, J.-G. Ren, W.-Q. Cai, W.-Y. Liu, S.-L. Li, R. Shu, Y.-M. Huang, L. Deng, L. Li, Q. Zhang, N.-L. Liu, Y.-A. Chen, C.-Y. Lu, X.-B. Wang, F. Xu, J.-Y. Wang, C.-Z. Peng, A. K. Ekert, and J.-W. Pan, Nature **582**, 501 (2020).
[14] S.-K. Liao, W.-Q. Cai, J. Handsteiner, B. Liu, J. Yin, L. Zhang, D. Rauch, M. Fink, J.-G. Ren, W.-Y. Liu, Y. Li, Q. Shen, Y. Cao, F.-Z. Li, J.-F. Wang, Y.-M. Huang, L. Deng, T. Xi, L. Ma, T. Hu, L. Li, N.-L. Liu, F. Koidl, P. Wang, Y.-A. Chen, X.-B. Wang, M. Steindorfer, G. Kirchner, C.-Y. Lu, R. Shu, R. Ursin, T. Scheidl, C.-Z. Peng, J.-Y. Wang, A. Zeilinger, and J.-W. Pan, Phys. Rev. Lett. **120**, 030501 (2018).
[15] Y.-A. Chen, Q. Zhang, T.-Y. Chen, W.-Q. Cai, S.-K. Liao, J. Zhang, K. Chen, J. Yin, J.-G. Ren, Z. Chen, S.-L. Han, Q. Yu, K. Liang, F. Zhou, X. Yuan, M.-S. Zhao, T.-Y. Wang, X. Jiang, L. Zhang, W.-Y. Liu, Y. Li, Q. Shen, Y. Cao, C.-Y. Lu, R. Shu, J.-Y. Wang, L. Li, N.-L. Liu, F. Xu, X.-B. Wang, C.-Z. Peng, and J.-W. Pan, Nature **589**, 214 (2021).
[16] T. Vergoossen, S. Loarte, R. Bedington, H. Kuiper, and A. Ling, Acta Astronaut. **173**, 164 (2020).

[17] K. Boone, J.-P. Bourgoin, E. Meyer-Scott, K. Heshami, T. Jennewein, and C. Simon, Phys. Rev. A **91**, 052325 (2015).

[18] C. Liorni, H. Kampermann, and D. Bruß, New Journal of Physics **23**, 053021 (2021).

[19] M. Gündoğan, J. S. Sidhu, V. Henderson, L. Mazzarella, J. Wolters, D. K. L. Oi, and M. Krutzik, npj Quant. Inf. **7**, 128 (2021).

[20] E. Da Ros, S. Kanthak, E. Sağlamyürek, M. Gündoğan, and M. Krutzik, "Proposal for a long-lived quantum memory using matter-wave optics with bose-einstein condensates in microgravity," (2022), arXiv:2210.13859.

[21] J. Wallnöfer, F. Hahn, M. Gündoğan, J. S. Sidhu, F. Wiesner, N. Walk, J. Eisert, and J. Wolters, Communications Physics **5**, 169 (2022).

[22] W. Li, P. Islam, and P. Windpassinger, Phys. Rev. Lett. **125**, 150501 (2020).

[23] S. J. Devitt, A. D. Greentree, A. M. Stephens, and R. Van Meter, Scientific Reports **6**, 36163 (2016).

[24] S. E. Wittig, S. M. Wittig, A. Berquanda, M. Zhong, and M. J. Sellars, "Concept for single-satellite global quantum key distribution using a solid state quantum memory," `http://iafastro.directory/iac/paper/id/36863/summary/` (2017), IAC-17,B2,7,1,x36863.

[25] J. Bland-Hawthorn, M. J. Sellars, and J. G. Bartholomew, J. Opt. Soc. Am. B **38**, A86 (2021).

[26] D. Luong, L. Jiang, J. Kim, and N. Lütkenhaus, Appl. Phys. B **122**, 96 (2016).

[27] R. Trényi and N. Lütkenhaus, Phys. Rev. A **101**, 012325 (2020).

[28] S. Langenfeld, P. Thomas, O. Morin, and G. Rempe, Phys. Rev. Lett. **126**, 230506 (2021).

[29] J. V. Rakonjac, D. Lago-Rivera, A. Seri, M. Mazzera, S. Grandi, and H. de Riedmatten, Phys. Rev. Lett. **127**, 210502 (2021).

[30] S. Pirandola, U. L. Andersen, L. Banchi, M. Berta, D. Bunandar, R. Colbeck, D. Englund, T. Gehring, C. Lupo, C. Ottaviani, J. L. Pereira, M. Razavi, J. S. Shaari, M. Tomamichel, V. C. Usenko, G. Vallone, P. Villoresi, and P. Wallden, Adv. Opt. Photon. **12**, 1012 (2020).

[31] C. C.-W. Lim, F. Xu, J.-W. Pan, and A. Ekert, Phys. Rev. Lett. **126**, 100501 (2021).

[32] M. U. Staudt, M. Afzelius, H. de Riedmatten, S. R. Hastings-Simon, C. Simon, R. Ricken, H. Suche, W. Sohler, and N. Gisin, Phys. Rev. Lett. **99**, 173602 (2007).

[33] M. Gündoğan, M. Mazzera, P. M. Ledingham, M. Cristiani, and H. de Riedmatten, New Journal of Physics **15**, 045012 (2013).

[34] Y. Ma, Y.-Z. Ma, Z.-Q. Zhou, C.-F. Li, and G.-C. Guo, Nat. Commun. **12**, 2381 (2021).

[35] M. Afzelius, C. Simon, H. de Riedmatten, and N. Gisin, Phys. Rev. A **79**, 052329 (2009).

[36] M. Zhong, M. P. Hedges, R. L. Ahlefeldt, J. G. Bartholomew, S. E. Beavan, S. M. Wittig, J. J. Longdell, and M. J. Sellars, Nature **517**, 177 (2015).

[37] According to Ref. [31, 60], when corrected, this corresponds to a larger security parameter of around 10^{-9}.

[38] Y.-F. Pu, N. Jiang, W. Chang, H.-X. Yang, C. Li, and L.-M. Duan, Nat. Commun. **8**, 15359 (2017).

[39] A. Seri, D. Lago-Rivera, A. Lenhard, G. Corrielli, R. Osellame, M. Mazzera, and H. de Riedmatten, Phys. Rev. Lett. **123**, 080502 (2019).

[40] P. Goldner, A. Ferrier, and O. Guillot-Noël, *Chapter 267 - Rare Earth-Doped Crystals for Quantum Information Processing*, edited by J.-C. G. Bünzli and V. K. Pecharsky, Handbook on the Physics and Chemistry of Rare Earths, Vol. 46 (Elsevier, 2015) pp. 1–78.

[41] F. Könz, Y. Sun, C. W. Thiel, R. L. Cone, R. W. Equall, R. L. Hutcheson, and R. M. Macfarlane, Phys. Rev. B **68**, 085109 (2003).

[42] B. Lauritzen, N. Timoney, N. Gisin, M. Afzelius, H. de Riedmatten, Y. Sun, R. M. Macfarlane, and R. L. Cone, Phys. Rev. B **85**, 115111 (2012).

[43] J. V. Rakonjac, G. Corrielli, D. Lago-Rivera, A. Seri, M. Mazzera, S. Grandi, R. Osellame, and H. de Riedmatten, Science Advances **8**, eabn3919 (2022), https://www.science.org/doi/pdf/10.1126/sciadv.abn3919.

[44] D.-C. Liu, P.-Y. Li, T.-X. Zhu, L. Zheng, J.-Y. Huang, Z.-Q. Zhou, C.-F. Li, and G.-C. Guo, Phys. Rev. Lett. **129**, 210501 (2022).

[45] M.-X. Su, T.-X. Zhu, C. Liu, Z.-Q. Zhou, C.-F. Li, and G.-C. Guo, Phys. Rev. A **105**, 052432 (2022).

[46] N. Sinclair, E. Saglamyurek, H. Mallahzadeh, J. A. Slater, M. George, R. Ricken, M. P. Hedges, D. Oblak, C. Simon, W. Sohler, and W. Tittel, Phys. Rev. Lett. **113**, 053603 (2014).

[47] G. Corrielli, A. Seri, M. Mazzera, R. Osellame, and H. de Riedmatten, Phys. Rev. Applied **5**, 054013 (2016).

[48] J. R. Olson, P. Champagne, E. Roth, T. Nast, E. Saito, V. Loung, A. C. Kenton, and C. L. Dobbins, AIP Conference Proceedings **1573**, 357 (2014).

[49] L. You, J. Quan, Y. Wang, Y. Ma, X. Yang, Y. Liu, H. Li, J. Li, J. Wang, J. Liang, Z. Wang, and X. Xie, Opt. Express **26**, 2965 (2018).

[50] H. Dang, T. Zhang, R. Zha, J. Tan, J. Li, Y. Zhao, B. Zhao, H. Tan, and R. Xue, IEEE Transactions on Applied Superconductivity **29**, 1 (2019).

[51] R. Barzel, M. Gündoğan, M. Krutzik, D. Rätzel, and C. Lämmerzahl, "Gravitationally induced entanglement dynamics of photon pairs and quantum memories," (2022), arXiv:2209.02099.

[52] M. Gündoğan, T. Jennewein, F. K. Asadi, E. D. Ros, E. Sağlamyürek, D. Oblak, T. Vogl, D. Rieländer, J. Sidhu, S. Grandi, L. Mazzarella, J. Wallnöfer, P. Ledingham, L. LeBlanc, M. Mazzera, M. Mohageg, J. Wolters, A. Ling, M. Atatüre, H. de Riedmatten, D. Oi, C. Simon, and M. Krutzik, "Topical white paper: A case for quantum memories in space," (2021), arXiv:2111.09595.

[53] J.-M. Mol, L. Esguerra, M. Meister, D. E. Bruschi, A. W. Schell, J. Wolters, and L. Wörner, Quantum Science and Technology **8**, 024006 (2023).

[54] M. Gündoğan, P. M. Ledingham, K. Kutluer, M. Mazzera, and H. de Riedmatten, Phys. Rev. Lett. **114**, 230501 (2015).

[55] A. Ortu, A. Holzäpfel, J. Etesse, and M. Afzelius, npj Quantum Information **8**, 29 (2022).

[56] L. Heller, J. Lowinski, K. Theophilo, A. Padrón-Brito, and H. de Riedmatten, Phys. Rev. Appl. **18**, 024036 (2022).

[57] M. Er-long, H. Zheng-fu, G. Shun-sheng, Z. Tao, D. Dasheng, and G. Guang-can, New Journal of Physics **7**, 215 (2005).

[58] M. Abasifard, C. Cholsuk, R. G. Pousa, A. Kumar, A. Zand, T. Riel, D. K. L. Oi, and T. Vogl, "The ideal wavelength for daylight free-space quantum key distribu-

tion," (2023), arXiv:2303.02106.

[59] X. Ma, C.-H. F. Fung, and H.-K. Lo, Phys. Rev. A **76**, 012307 (2007).
[60] M. Tomamichel and A. Leverrier, Quantum **1**, 14 (2017).